



Identifying the biological control of the interannual and long-term variations in South Atlantic air-sea CO₂ flux

Daniel J. Ford^{1,2}, Gavin H. Tilstone¹, Jamie D. Shutler² and Vassilis Kitidis¹

¹ Plymouth Marine Laboratory, Plymouth, UK

5 ² College of Life and Environmental Sciences, University of Exeter, Penryn, UK

Correspondence to: Daniel Ford (dfo@pml.ac.uk)

Abstract. The accumulation of anthropogenic CO₂ emissions in the atmosphere has been buffered by the global oceans absorbing CO₂ and acting as a net CO₂ sink. The CO₂ flux between the atmosphere and the ocean, that collectively results in the oceanic carbon sink, is spatially and temporally variable, and fully understanding the driving mechanisms behind this
10 flux is key to assessing how the sink may change in the future. In this study a time series decomposition analysis was applied to satellite observations to determine the drivers that control the sea-air difference of CO₂ partial pressure ($\Delta p\text{CO}_2$) and the CO₂ flux on seasonal and interannual time scales in the South Atlantic Ocean. Linear trends in $\Delta p\text{CO}_2$ and the CO₂ flux were calculated to identify key areas of change.

Seasonally, changes in both the $\Delta p\text{CO}_2$ and CO₂ flux were dominated by sea surface temperature (SST) in the subtropics
15 (north of 40 °S) and correlated with biological processes in the subpolar regions (south of 40 °S). The Equatorial Atlantic indicated that biological processes were a key driver, as a response to upwelling and riverine inputs. These results highlighted that seasonally $\Delta p\text{CO}_2$ can act as an indicator to identify drivers of the CO₂ flux. Interannually, the SST and biological contributions to the CO₂ flux in the subtropics were correlated with the Multivariate ENSO Index (MEI) leading to a weaker (stronger) CO₂ sink in El Niño (La Niña) years.

20 The 16-year time-series identified significant trends in $\Delta p\text{CO}_2$ and CO₂ flux, however, these trends were not always consistent in magnitude or spatial extent. Therefore, predicting the oceanic response to climate change requires the examination of CO₂ flux rather than $\Delta p\text{CO}_2$. Positive CO₂ flux trends (weakening sink for atmospheric CO₂) were identified within the Benguela upwelling system, consistent with increased upwelling and wind speeds. Negative trends in the CO₂ flux (intensifying sink for atmospheric CO₂) offshore into the South Atlantic Gyre, were consistent with an increase in the export
25 of nutrients in mesoscale features, which drive biological drawdown of CO₂. These long-term trends in the CO₂ flux indicate that the biological contribution to changes in the air-sea CO₂ flux cannot be overlooked when scaling up to estimates of the global ocean carbon sink.



1 Introduction

30 Since the industrial revolution, anthropogenic CO₂ emissions have increased unabated and continue to rise atmospheric CO₂ concentrations (IPCC, 2021). The global oceans have buffered the rise by sequestering CO₂ from the atmosphere at a rate between 1 and 3.5 Pg C yr⁻¹ (e.g. Friedlingstein et al., 2020; Landschützer et al., 2014; Watson et al., 2020). The strength of the ocean as a sink for CO₂ appears to be increasing with time (Friedlingstein et al., 2020; Watson et al., 2020). Regionally this can vary hugely, however and the ocean can oscillate between a source or sink of atmospheric CO₂. The difference in the partial pressure of CO₂ ($p\text{CO}_2$) between the seawater and atmosphere ($\Delta p\text{CO}_2$) is used as an indicator or proxy, for the
35 net direction of air-sea CO₂ flux during gas exchange.

In the open ocean, changes in physical and biogeochemical processes that control seawater $p\text{CO}_2$ ($p\text{CO}_2(\text{sw})$) also modify $\Delta p\text{CO}_2$ as the atmospheric $p\text{CO}_2$ ($p\text{CO}_2(\text{atm})$) is by comparison less variable (e.g. Henson et al., 2018; Landschützer et al., 2016). $\Delta p\text{CO}_2$ can therefore be controlled by changes in sea surface temperature (SST) because the solubility of CO₂ is inversely proportional to the temperature (Weiss, 1974). In addition, plankton net community production (NCP) modifies the
40 concentration of CO₂ in the seawater depending on the balance between net primary production (NPP; uptake of CO₂ via photosynthesis) and respiration (release of CO₂ into the water). The NCP describes the overall metabolic balance of the plankton community, where positive (negative) NCP indicates a drawdown (or release) of CO₂ from (or into) the water contributing to a decrease (increase) in $\Delta p\text{CO}_2$. Physical processes, including riverine input (e.g. Ibáñez et al., 2016; Lefèvre et al., 2020; Valerio et al., 2021), and upwelling (e.g. González-Dávila et al., 2009; Lefèvre et al., 2008; Santana-
45 Casiano et al., 2009) can alter $p\text{CO}_2(\text{sw})$ and $\Delta p\text{CO}_2$ directly through the entrainment of high-CO₂ water or indirectly by modifying NCP through nutrient supply (enhancing photosynthesis) and or organic material supply (enhancing respiration).

The air-sea CO₂ flux is more precisely a function of the difference in CO₂ concentrations across the mass boundary layer however, with any turbulent exchange characterised by the gas exchange coefficient. The CO₂ concentration difference is determined by the $p\text{CO}_2$ at the base ($p\text{CO}_2(\text{sw})$) and top ($p\text{CO}_2(\text{atm})$) of the boundary layer and the respective solubilities
50 (Weiss, 1974), which must be carefully calculated due to vertical temperature gradients existing across the mass boundary layer (Woolf et al., 2016). The gas exchange coefficient is usually parameterised as a function of wind speed (e.g. Ho et al., 2006; Nightingale et al., 2000; Wanninkhof, 2014) which accounts for ~75% of the variance in surface turbulent exchange (e.g. Dong et al., 2021; Ho et al., 2006). Therefore, clearly both oceanographic and meteorological conditions are able to modify and control the seasonality, interannual variability and long-term trends of this flux.

55 Seasonal drivers of $\Delta p\text{CO}_2$ have been explored globally (Takahashi et al., 2002), and regionally in the Atlantic Ocean (Henson et al., 2018; Landschützer et al., 2013). Takahashi et al. (2002) binned *in situ* $p\text{CO}_2(\text{sw})$ observations to a 4° by 5° grid globally, and reported that SST drives $\Delta p\text{CO}_2$ in the subtropics, and non-temperature processes (i.e. biological activity and ocean circulation) dominate in subpolar and equatorial regions. Landschützer et al. (2013) used a self-organising map feed forward neural network (SOM-FNN) technique to extrapolate the *in situ* $p\text{CO}_2(\text{sw})$ observations and reported similar
60 seasonal drivers in the Atlantic Ocean with one exception, that temperature and non-temperature processes compensated



each other in the Equatorial Atlantic. Henson et al. (2018) using binned *in situ* observations for the North Atlantic Ocean, also indicated that the subtropics are driven by SST and that subpolar regions are correlated with biological activity. The interannual drivers of $\Delta p\text{CO}_2$ are different compared to the seasonal drivers in the North Atlantic (Henson et al., 2018), which could be true of the South Atlantic Ocean, though this needs to be further investigated. Landschützer et al. (2014, 65 2016) postulated the El Niño cycle may influence $\Delta p\text{CO}_2$ in the subtropical South Atlantic but did not explore the underlying processes. South of 35° S, Landschützer et al. (2015) indicated that atmospheric forcing could control interannual variability of $\Delta p\text{CO}_2$ through changes in Ekman transport and upwelling. These interannual drivers of $\Delta p\text{CO}_2$ and the CO_2 flux in the South Atlantic Ocean are poorly understood but have key implications for determining how the oceanic CO_2 sink could be impacted by climate change and its evolution over interannual and decadal timescales.

70 In this study, we investigate the drivers of $\Delta p\text{CO}_2$ and the CO_2 flux in the South Atlantic Ocean over both seasonal and interannual timescales using a timeseries decomposition approach. Trends in $\Delta p\text{CO}_2$ and the CO_2 flux were calculated from 2002 to 2018, and regions in the South Atlantic Ocean showing the greatest change in the CO_2 flux are investigated.

2. Data and Methods

2.1. $p\text{CO}_2$ data

75 Satellite estimates of $p\text{CO}_2$ (sw) were retrieved from the South Atlantic Feed Forward Neural Network (SA-FNN) dataset (Ford et al., 2021b, 2022). Ford et al. (2022) showed that the SA-FNN improved on the seasonal $p\text{CO}_2$ (sw) variability in the South Atlantic Ocean compared to current estimates using the ‘state of the art’ methodology (the SOM-FNN). The SA-FNN estimates $p\text{CO}_2$ (sw) by clustering *in situ* monthly 1° gridded Surface Ocean CO_2 Atlas (SOCAT) v2020 $p\text{CO}_2$ (sw) observations (Bakker et al., 2016; Sabine et al., 2013), that have been reanalysed into a dataset configured using consistent depth and 80 temperature fields (Goddijn-Murphy et al., 2015; Reynolds et al., 2002; Woolf et al., 2016), into eight static provinces in the South Atlantic Ocean. The nonlinear relationships between $p\text{CO}_2$ (sw) and three environmental drivers; SST, NCP and $p\text{CO}_2$ (atm) were constructed for each province with a feed forward neural network (FNN). The FNN for each province were applied to produce spatially and temporally complete $p\text{CO}_2$ (sw) fields on monthly 1° grids between July 2002 and December 2018, with uncertainties also generated on a per pixel basis as described in Ford et al. (2022).

85 Monthly 1° grids of $p\text{CO}_2$ (atm) were extracted from v5.5 of the global estimates of $p\text{CO}_2$ (sw) dataset (Landschützer et al., 2016, 2017). $p\text{CO}_2$ (atm) was estimated using the dry mixing ratio of CO_2 from the NOAA-ESRL marine boundary layer reference (<https://www.esrl.noaa.gov/gmd/ccgg/mb/>; last accessed 25/09/2020), Optimum Interpolated SST (Reynolds et al., 2002) and sea level pressure following Dickson et al. (2007). $\Delta p\text{CO}_2$ was calculated from $p\text{CO}_2$ (sw) and $p\text{CO}_2$ (atm) as;

$$\Delta p\text{CO}_2 = p\text{CO}_2(\text{sw}) - p\text{CO}_2(\text{atm}) \quad (1)$$

90 2.2. Air-sea CO_2 flux data

The air-sea CO_2 flux (F) can be estimated using a bulk parameterisation as:



$$F = k (\alpha_w pCO_2 (sw) - \alpha_s pCO_2 (atm)) \quad (2)$$

Where k is the gas transfer velocity which was estimated from ERA5 monthly reanalysis wind speed (Hersbach et al., 2019) following the parameterisation of Nightingale et al. (2000). α_w and α_s are the solubility of CO_2 at the base and top of the mass boundary layer at the sea surface (Woolf et al., 2016). α_w was calculated as a function of SST and sea surface salinity (Weiss, 1974) using the monthly Optimum Interpolated SST (Reynolds et al., 2002) and sea surface salinity from the Copernicus Marine Environment Modelling Service global ocean physics reanalysis product (GLORYS12V1; CMEMS, 2021). α_s was calculated using the same temperature and salinity datasets but included a gradient from the base to the top of mass boundary layer of -0.17 K (Donlon et al., 1999) and $+0.1$ salinity units (Woolf et al., 2016). $pCO_2 (atm)$ was calculated using the dry mixing ratio of CO_2 from the NOAA-ESRL marine boundary layer reference, Optimum Interpolated SST (Reynolds et al., 2002) applying a cool skin bias (0.17 K; Donlon et al., 1999) and sea level pressure following Dickson et al. (2007).

All of these calculations along with the resulting monthly CO_2 flux were carried out using the open source FluxEngine toolbox (Holding et al., 2019; Shutler et al., 2016), for the period between July 2002 and December 2018, assuming ‘rapid’ transfer (as described in Woolf et al., 2016).

105 2.3. Biological data

The 4 km resolution mean monthly Chl a was calculated from Moderate Resolution Imaging Spectroradiometer on Aqua (MODIS-A) Level 1 granules, retrieved from the National Aeronautics Space Administration (NASA) Ocean Colour website (<https://oceancolor.gsfc.nasa.gov/>; last accessed 10/12/2020), using SeaDAS v7.5, and applying the standard OC3-CI algorithm for Chl a (https://oceancolor.gsfc.nasa.gov/atbd/chlor_a/; last accessed 15/12/2020). Monthly composites of MODIS-A SST (NASA OBPG, 2015) and photosynthetically active radiation (PAR; NASA OBPG, 2017b) were also downloaded from the NASA Ocean Colour website. Monthly NPP composites were generated from MODIS-A Chl a , SST and PAR composites using the Wavelength Resolving Model (Morel, 1991) with the look up table described in Smyth et al. (2005). Coincident monthly composites of NCP using the algorithm NCP-D described in Tilstone et al. (2015) were generated using the NPP and SST data. Further details of the satellite algorithms are given in O’Reilly et al. (1998), O’Reilly and Werdell (2019) and Hu et al. (2012) for Chl a , Smyth et al. (2005), Tilstone et al. (2005, 2009) for NPP and Tilstone et al. (2015) for NCP. Monthly composites were generated between July 2002 and December 2018 and were re-gridded onto the same 1° grid as the $pCO_2 (sw)$ and flux data. Ford et al. (2021a) showed that these satellite algorithms for Chl a , NPP, NCP and SST are accurate compared to *in situ* observations in the South Atlantic Ocean following an algorithm intercomparison which accounted for model, *in situ* and input parameter uncertainties.

120 2.4. Seasonal and interannual driver analysis

An X-11 analysis (Pezzulli et al., 2005; Shiskin et al., 1967) was performed following the approach described by Henson et al. (2018), on a per pixel basis using monthly 1° fields of ΔpCO_2 that were estimated from $pCO_2 (atm)$ and SA-FNN $pCO_2 (sw)$. The spatially and temporally varying $pCO_2 (sw)$ uncertainty was propagated through the X-11 analysis, using a Monte Carlo



uncertainty propagation approach. The input time series were randomly perturbed 1000 times within the uncertainty of each
125 $p\text{CO}_2$ (sw) estimate, and Spearman correlations calculated for each perturbation. The 95% confidence interval was extracted
from the resulting distribution of correlations coefficients, and results were deemed significant ($\alpha < 0.05$) where the
confidence interval remained significant. Spatial autocorrelation was tested using the method of field significance (Wilks,
2006).

The potential drivers tested were MODIS-A SST, NCP and NPP alongside three climate indices: the North Atlantic
130 Oscillation (NAO), indicating the atmospheric condition over the North Atlantic Ocean, downloaded from
<http://www.cgd.ucar.edu/cas/catalog/> (last accessed: 31/12/2019); Multivariate ENSO Index (MEI) as an indicator of El
Niño Southern Oscillation phases, <https://www.esrl.noaa.gov/psd/enso/mei> (last accessed: 19/12/2019); Southern Annular
Mode (SAM) data, which indicate the displacement of the westerly winds in the Southern Ocean, were downloaded from
<http://www.nerc-bas.ac.uk/icd/gjma/sam.html> (last accessed: 19/12/2019).

135 The X-11 analysis was then conducted on the CO_2 fluxes, on a per pixel basis. The $p\text{CO}_2$ (sw) and gas transfer uncertainties
were propagated through the flux calculations using the same Monte Carlo uncertainty propagation approach used for
 $\Delta p\text{CO}_2$. The uncertainty in the gas transfer coefficient was assumed to be $\pm 10\%$ (Woolf et al., 2019).

It should be noted that correlations between the $\Delta p\text{CO}_2$ and SST/NCP are expected since the SA-FNN estimates $p\text{CO}_2$ (sw)
(the major determinant of $\Delta p\text{CO}_2$ variability) using SST and NCP as input parameters which are subsequently interpreted as
140 drivers here. By extension, but to a lesser extent, this also applies to correlations between CO_2 flux and SST/NCP since $p\text{CO}_2$
(sw) is included in the flux calculations. Different lines of evidence suggest that this is not a major limitation of our study.
Firstly, any correlation between $\Delta p\text{CO}_2/\text{CO}_2$ flux and SST/NCP is not determined *a priori*, but is an emerging property of the
SA-FNN. Therefore, the driver analysis undertaken here represents an indirect decomposition of the SA-FNN drivers rather
than a strict correlation analysis between independent variables. The accurate representation of seasonal $p\text{CO}_2$ (sw) cycles
145 across the South Atlantic Ocean (Ford et al., 2022) provides confidence in the SA-FNN. Secondly, conducting the analysis
described by Henson et al. (2018) using *in situ* $p\text{CO}_2$ (sw) to estimate $\Delta p\text{CO}_2$ on a per province basis (Longhurst, 1998),
yielded similar drivers (Appendix A).

2.5. Trend analysis

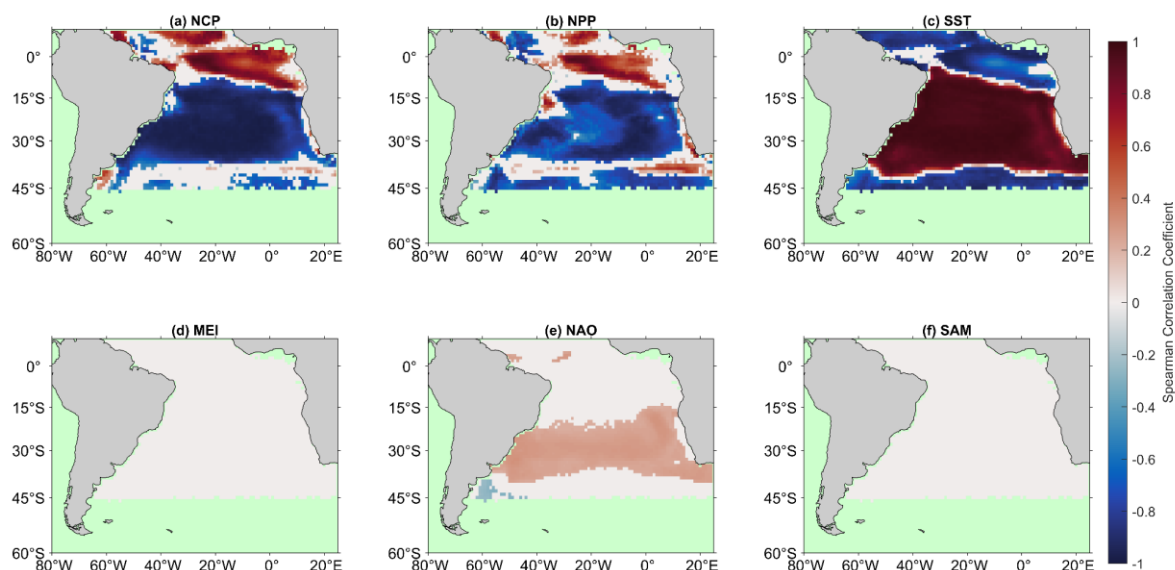
The linear trend in the interannual components of $\Delta p\text{CO}_2$ and the CO_2 flux were calculated on a per pixel basis using the non
150 parametric Mann-Kendall test for trend (Kendall, 1975; Mann, 1945) and Sen's Slope estimates (Sen, 1968), which are less
sensitive to outliers in the timeseries. The $p\text{CO}_2$ (sw) and gas transfer coefficient uncertainties were propagated within this
trend analysis using a Monte Carlo uncertainty propagation ($n = 1000$) in order to extract the 95% confidence interval on the
trends. The overall trend was deemed significant if 95% of the trends were significant ($\alpha = 0.05$).



3. Results

155 3.1. Seasonal drivers of $\Delta p\text{CO}_2$ and CO_2 flux

The X-11 analysis conducted on $\Delta p\text{CO}_2$ indicated significant seasonal correlations (Fig. 1), when the uncertainties are accounted for. The subtropics (10 °S to 40 °S) showed positive correlations between $\Delta p\text{CO}_2$ and SST (Fig. 1c), as well as negative correlations between $\Delta p\text{CO}_2$, NCP and NPP (Fig. 1a, b). In contrast the subpolar (south of 40 °S) and equatorial regions (10 °N to 10 °S) displayed negative correlations between $\Delta p\text{CO}_2$ and SST (Fig. 1c). Correlations between $\Delta p\text{CO}_2$ and NCP were negative in the subpolar regions and were positive in the Equatorial regions (Fig. 1a). The correlation between $\Delta p\text{CO}_2$ and NCP in the equatorial region was greater than between $\Delta p\text{CO}_2$ and NPP (Fig. 1a, b). There were no significant correlations observed between $\Delta p\text{CO}_2$ and MEI, NAO or SAM in any of the regions.



165 **Figure 1: Significant Spearman correlations between the $\Delta p\text{CO}_2$ seasonal component of the X-11 analysis and (a) net community production, (b) net primary production, (c) sea surface temperature, (d) Multivariate ENSO index, (e) North Atlantic Oscillation and (f) Southern Annular Mode seasonal components. White regions indicate no significant correlations, and green regions indicate no analysis was performed due to missing satellite data.**

170 Regional deviations were observed in the Amazon Plume and Benguela upwelling. The region under the influence of the Amazon Plume indicated negative correlations between $\Delta p\text{CO}_2$ and NCP in contrast to the surrounding positive correlations (Fig. 1a). The Benguela upwelling displayed positive correlations between $\Delta p\text{CO}_2$ and NCP (Fig. 1a) and no significant correlations between $\Delta p\text{CO}_2$ and SST (Fig. 1c). Performing the X-11 analysis on the CO_2 flux revealed similar and



comparable correlations to $\Delta p\text{CO}_2$ (Fig. 2). Significant driver-flux correlations were observed over a larger area however,
175 compared to $\Delta p\text{CO}_2$.

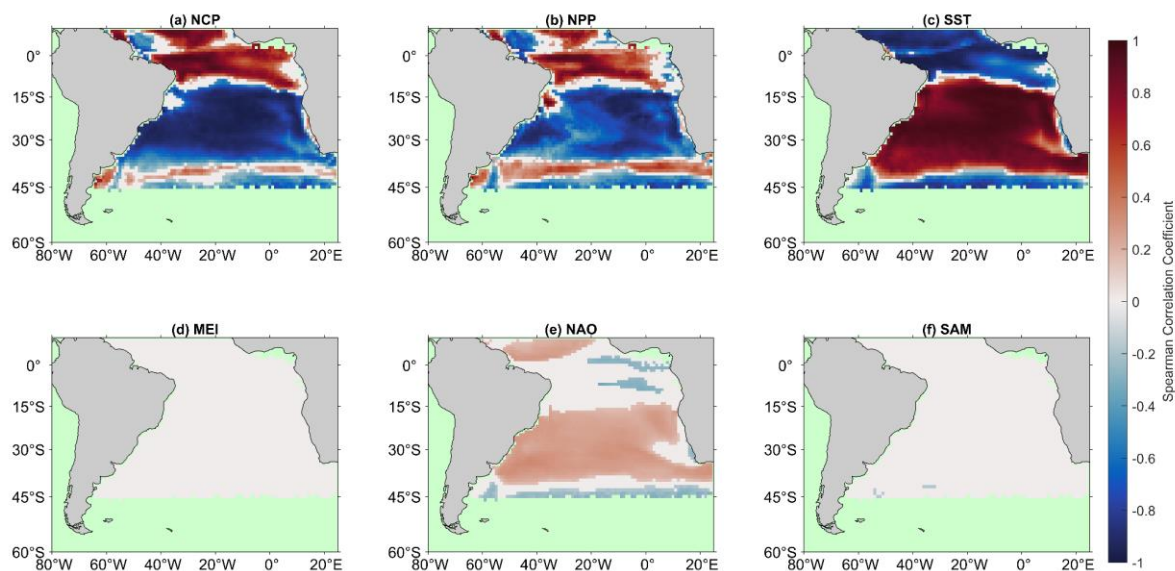
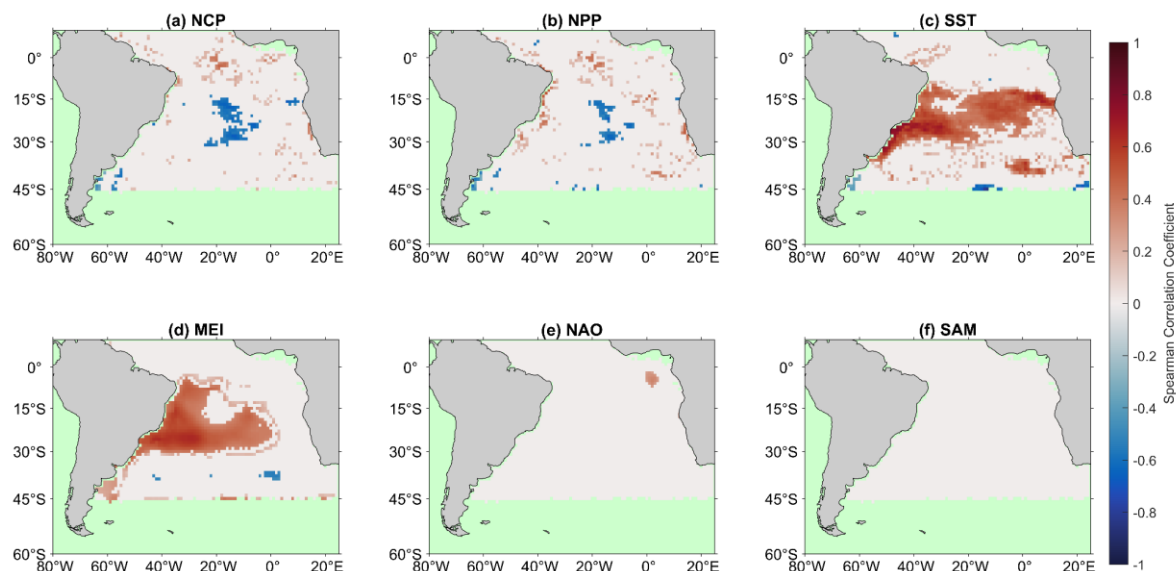


Figure 2: Significant Spearman correlations between the air-sea CO_2 flux seasonal component of the X-11 analysis and (a) net community production, (b) net primary production, (c) sea surface temperature, (d) Multivariate ENSO index, (e) North Atlantic Oscillation and (f) Southern Annular Mode seasonal components. White regions indicate no significant correlations, and green regions indicate no analysis was performed due to missing satellite data.
180

3.2. Interannual drivers of $\Delta p\text{CO}_2$ and CO_2 flux

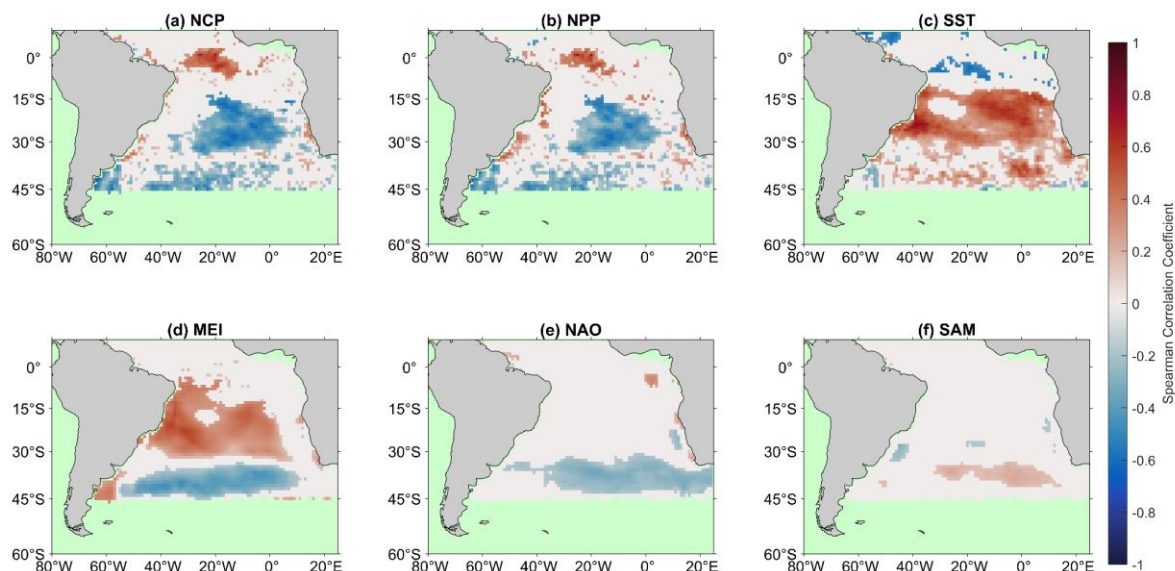
The X-11 analysis identified regionally significant interannual correlations between $\Delta p\text{CO}_2$ and SST, MEI and to a lesser extent NCP (Fig. 3). The subtropics displayed positive correlations between SST and $\Delta p\text{CO}_2$, which extended across the basin from the South American coast (Fig. 3c). Positive correlations were also observed between the MEI and $\Delta p\text{CO}_2$ (Fig. 3d), with a similar geographic extent as the correlations with SST. In the central South Atlantic gyre spatially variable negative correlations between NCP and $\Delta p\text{CO}_2$ were observed (Fig. 3a). The central Equatorial Atlantic displayed spatially variable positive correlations between NCP and $\Delta p\text{CO}_2$, which extended south-east towards the African coast (Fig. 3a).
185



190 **Figure 3: Significant Spearman correlations between the $\Delta p\text{CO}_2$ interannual component of the X-11 analysis and (a) net community production, (b) net primary production, (c) sea surface temperature, (d) Multivariate ENSO index, (e) North Atlantic Oscillation and (f) Southern Annular Mode interannual components. White regions indicate no significant correlations, and green regions indicate no analysis was performed due to missing satellite data.**

195 Significant interannual correlations for the CO_2 flux were also identified by the X-11 analysis (Fig. 4), which generally covered a larger spatial area to the corresponding $\Delta p\text{CO}_2$ correlations (Fig. 3). Positive correlations between the CO_2 flux and SST were observed in the subtropics (Fig. 4c), consistent with the $\Delta p\text{CO}_2$ correlations (i.e. by comparing Fig. 4c and Fig. 3c). Nevertheless, negative correlations between the CO_2 flux and SST were observed at the border between the equatorial region and subtropics; a feature that was not identified in the $\Delta p\text{CO}_2$ correlations. Negative correlations between
200 NCP and the CO_2 flux were also identified over a spatially larger area (Fig. 4a, 3a). Correlations between the MEI and CO_2 flux were positive in the subtropics (Fig. 4d) and included a band of negative correlations to the south between 35 °S and 45 °S (Fig. 4d).

Positive correlations between NCP and CO_2 flux were observed in the western equatorial Atlantic, alongside spatially variable negative correlations to SST (Fig. 4a, c). Weak positive correlations between the SAM and CO_2 flux were identified
205 between 30° S and 45° S (Fig. 4f), as well as weak negative correlations between the CO_2 flux and NAO (Fig. 4e).



210 **Figure 4: Significant Spearman correlations between the air-sea CO₂ flux interannual component of the X-11 analysis and (a) net community production, (b) net primary production, (c) sea surface temperature, (d) Multivariate ENSO index, (e) North Atlantic Oscillation and (f) Southern Annular Mode interannual components. White regions indicate no significant correlations, and green regions indicate no analysis was performed due to missing satellite data.**

3.3. Trends in interannual $\Delta p\text{CO}_2$ and CO₂ flux

215 Connected regions of significant positive and negative trends in the interannual component of $\Delta p\text{CO}_2$ were observed across the region (Fig. 5a). Negative trends occurred in the South Atlantic gyre. Positive trends in $\Delta p\text{CO}_2$ were identified along the South African coast, which switched to strong negative trends moving offshore into the central South Atlantic gyre. Positive trends were also observed in the Equatorial Atlantic consistent with the positions of the Amazon Plume and Equatorial Upwelling.

220 Connected regions of significant positive and negative trends in the CO₂ flux were identified (Fig. 5b), but over much larger spatial areas than evident in the $\Delta p\text{CO}_2$ results (i.e. comparing Fig. 5a with 5b). The trends in CO₂ flux are generally in the same direction as trends in the $\Delta p\text{CO}_2$ results, however, the magnitude of the CO₂ flux trend is generally of lower magnitude. Strong positive trends in the CO₂ flux occurred in the Benguela upwelling region, before switching to a similar magnitude negative trend offshore with a greater spatial extent.

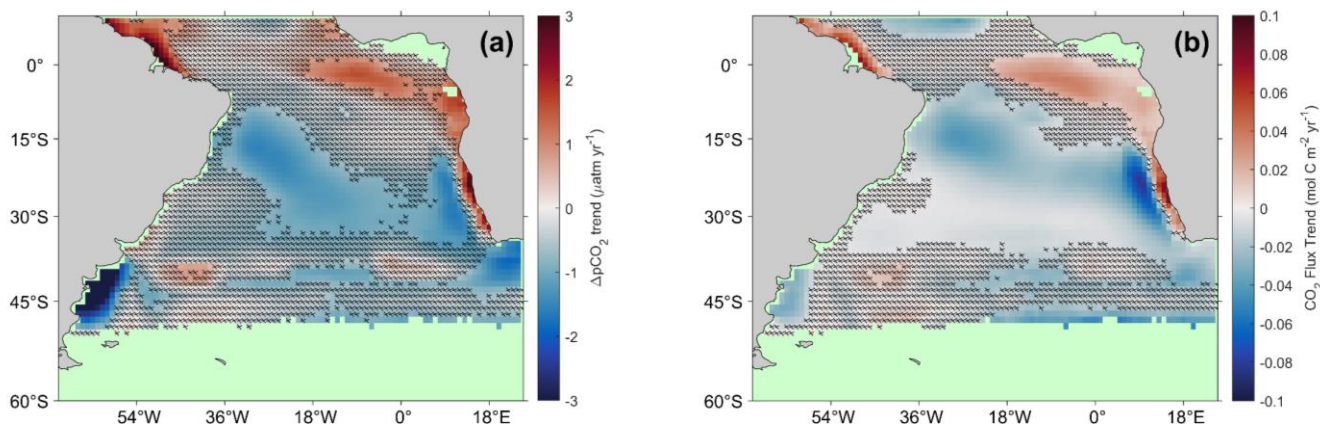


Figure 5: Linear trends in (a) $\Delta p\text{CO}_2$ and (b) the air-sea CO_2 flux between 2002 and 2018. Hashed areas indicate non-significant trends when accounting for the uncertainties. Green regions indicate insufficient data to calculate trends.

225 4. Discussion

4.1. Seasonal drivers of $\Delta p\text{CO}_2$ and CO_2 flux

Previous studies have explored the seasonal drivers of $\Delta p\text{CO}_2$ and to a lesser extent the air-sea CO_2 flux. In this study, we investigated the drivers of $\Delta p\text{CO}_2$ and CO_2 flux at both seasonal and interannual timescales in the South Atlantic Ocean. Henson et al. (2018) indicated that seasonal subtropical $\Delta p\text{CO}_2$ variability in the North Atlantic Ocean was driven by SST variability, while $\Delta p\text{CO}_2$ variability in subpolar regions was biologically driven, similar to previous studies (Landschützer et al., 2013; Takahashi et al., 2002). The X-11 analysis conducted here on spatially complete $\Delta p\text{CO}_2$ and CO_2 flux displayed consistent seasonal results (Fig. 1, 2), although the CO_2 flux produced a greater spatial area of significant correlations. These both indicated a similar pattern of seasonal drivers in the South Atlantic Ocean, with subtropical $\Delta p\text{CO}_2$ and CO_2 flux driven by SST, and subpolar correlated with biological controls, although the equatorial region displayed more complex drivers (Fig. 1).

In the Equatorial Atlantic, the correlations between $\Delta p\text{CO}_2$, temperature and biological production were spatially variable (Fig. 1). Landschützer et al. (2013) suggested that the temperature and non-temperature (i.e. biological and circulation) drivers generally compensated each other. We found positive correlations between NCP, $\Delta p\text{CO}_2$ and CO_2 flux seasonal components, indicating that biological activity was a key driver of seasonal variability in response to the equatorial upwelling and highlighting the dominance of non-temperature drivers. Ford et al. (2022) showed that the SA-FNN improved on the seasonal $p\text{CO}_2$ ($_{\text{sw}}$) variability in the Equatorial Atlantic compared to the current ‘state of the art’ SOM-FNN methodology (Watson et al., 2020). Elevated $\Delta p\text{CO}_2$ associated with elevated biological activity in the eastern Equatorial Atlantic was consistent with the seasonal equatorial upwelling (Radenac et al., 2020). Parard et al. (2010) indicated strong negative correlations between SST and $\Delta p\text{CO}_2$ during the upwelling season ($R^2 = -0.76$ for June to September), consistent



245 with our results. By contrast, Lefèvre et al. (2016) showed that correlations between $p\text{CO}_2$ (sw) and SST were weak across the whole year ($R^2 = -0.13$), and sea surface salinity was the primary driver at the same station.

In the western Equatorial Atlantic, negative correlations between NCP and $\Delta p\text{CO}_2$ seasonal components occurred in the vicinity of the Amazon River mouth. The mixing of the Amazon river and oceanic water decreases sea surface salinity (Bonou et al., 2016; Ibánhez et al., 2016; Lefèvre et al., 2010; Lefèvre et al., 2020), and increases the nutrient supply to the ocean which can enhance NPP and NCP, leading to a decrease in $\Delta p\text{CO}_2$ within the Amazon plume (Cooley et al., 2007; Körtzinger, 2003). This coupling produces an extensive area of depressed $\Delta p\text{CO}_2$ which is a CO_2 sink (Ibánhez et al., 2016). Lefèvre et al. (2010) indicated that rainfall from the intertropical convergence zone could reduce sea surface salinity, increasing CO_2 solubility in water, with an associated decrease in $\Delta p\text{CO}_2$. The Eastern Tropical Atlantic is also subject to large river input, especially from the Congo (Hopkins et al., 2013) and Niger rivers, which could produce nutrient-rich plumes that fuel NCP and decrease $\Delta p\text{CO}_2$ (Lefèvre et al., 2016, 2021).

Deviations from the expected drivers in the subtropics, occurred within the Benguela upwelling system between 20 °S and 35 °S. Positive correlations between NCP and the CO_2 flux (Fig. 2a) alongside negative correlations between SST and the CO_2 flux (Fig. 2c) are indicative of upwelled waters that have both elevated $p\text{CO}_2$ (sw) and nutrients, which cause an increase in NPP (Lamont et al., 2014). These upwelled waters move offshore in filaments (Rubio et al., 2009) where biological activity subsides, and SST becomes the dominant driver, reinforced by positive correlations between SST and the CO_2 flux further offshore. Ford et al. (2021a) indicated a switch in NCP drivers in the Benguela upwelling from wind driven upwelling on the shelf, to filaments that propagate offshore from the upwelling front, which is consistent with the switch in the drivers observed for the CO_2 flux moving offshore.

The seasonal correlations between the CO_2 flux and the drivers were similar to $\Delta p\text{CO}_2$, but for CO_2 flux these occurred over a larger spatial area. The South Atlantic subtropical anticyclone (Reboita et al., 2019) which controls wind speeds across the region, and therefore the gas transfer coefficient, could enhance the CO_2 flux into the subtropical ocean, through higher (or lower) wind speeds in winter (or summer; Xiong et al., 2015). Comparable results between $\Delta p\text{CO}_2$ and the CO_2 flux, would indicate that $\Delta p\text{CO}_2$ can be used as a proxy to understand seasonal variations in the CO_2 flux, because the seasonal variations in $\Delta p\text{CO}_2$ largely explain the seasonal variability in the CO_2 flux.

270 4.2. Interannual drivers of $\Delta p\text{CO}_2$ and CO_2 flux

The X-11 analytical econometric tool (Shiskin et al., 1967) has been shown to be effective in the decomposition of environmental time-series into their seasonal, interannual and residual components (Pezzulli et al., 2005; Vantrepotte & Mélin, 2011; Henson et al., 2018). The ability of the seasonal cycle to vary on a yearly basis in the X-11 approach, produces an interannual component that results in a robust representation of the longer-term changes in the timeseries.

275 The larger geographic region of significant correlations for the air-sea CO_2 flux compared to $\Delta p\text{CO}_2$, and the consistency between the two results (i.e. comparing the smaller regions of $\Delta p\text{CO}_2$ correlations with their equivalent in the flux results; Fig. 3, 4) suggests that analysing the CO_2 flux is the better dataset to investigate drivers of variations in inter-annual and



longer timescales. The results become clearer when analysing the CO₂ flux, where the effects of solubility and surface turbulence (estimated via wind speed proxy) could reinforce correlations and long-term trends, which will be retrieved by performing long timeseries analyses on the CO₂ flux. Landschutzer et al. (2015) showed that variations in the Southern Ocean carbon sink were primarily driven by changes in $\Delta p\text{CO}_2$, which may be the case when integrating across basin scales. At localised scales of 1° by 1° as performed in our analysis, changes in surface turbulence and solubility are shown to be important in determining interannual variability, consistent with Keppler and Landschützer (2019). Henson et al. (2018) showed that the seasonal and interannual drivers of $\Delta p\text{CO}_2$ were different in the North Atlantic Ocean, which could arise from the necessity to study CO₂ fluxes over longer timescales.

The interannual component of NCP and the CO₂ flux were negatively correlated in the subtropical gyre (Fig. 4a), alongside a positive correlation between SST and CO₂ flux (Fig. 4b). El Niño (La Niña) events are known to influence the South Atlantic Ocean, causing an increase (decrease) in SST across the basin (Colberg et al., 2004; Rodrigues et al., 2015), and a decrease (increase) in NPP and NCP (Ford et al., 2021a; Tilstone et al., 2015). Positive correlations between the MEI and CO₂ flux (Fig. 4d) indicates that the MEI partially controls the interannual variability in CO₂ flux in the South Atlantic subtropical gyre, through modulations primarily in SST and to a lesser extent NCP. The South Atlantic Subtropical Anticyclone has been observed to strengthen (weaken) and move south (north) during La Niña (El Niño) events. This displacement increases (decreases) wind speeds across the subtropical South Atlantic, which will enhance (weaken) gas exchange, and elevate (depress) NCP (Ford et al., 2021a). These results suggest a more significant role of biological activity in controlling the interannual variability in the CO₂ flux than previously thought.

The negative correlation between the CO₂ flux and the MEI in a band between 30° S and 45° S (Fig. 4d), indicates that reduced (elevated) wind speeds that occur during La Niña (El Niño) events in this region, suppress (enhance) the gas exchange (Colberg et al., 2004). In the equatorial region, neither $\Delta p\text{CO}_2$ or the CO₂ flux were correlated with the MEI, in sharp contrast with Lefevre et al. (2013) who showed stronger outgassing of CO₂ in the western equatorial Atlantic for the year following the 2009 El Niño. In that respect, it should be noted that our analysis would not identify such lagged correlations.

The SAM has known meteorological connections to the MEI (Fogt et al., 2011), where El Niño (La Niña) events generally coincide with negative (positive) SAM phases, resulting in northward (southward) displacement of the westerly winds in the Southern Ocean. Our results showed positive correlations between the CO₂ flux and the SAM between 30° S and 45° S (Fig. 4e) indicating stronger (weaker) CO₂ drawdown into the oceans during negative (positive) SAM phases. Although no significant correlations were found between $\Delta p\text{CO}_2$ and the SAM (Fig. 3e), the changes in the gas transfer driven by the displacement of the westerly winds could control the CO₂ flux. Landschützer et al. (2015) indicated that the SAM is unlikely to be the main driver of changes in the Southern Ocean CO₂ flux, but an observed zonally asymmetric atmospheric pattern could induce changes in the CO₂ flux (Keppler and Landschützer, 2019; Landschützer et al., 2015). This asymmetric atmospheric pattern, however, may not be captured within the SAM index.



4.3. Long term trends in $\Delta p\text{CO}_2$ and CO_2 flux

The trends in $\Delta p\text{CO}_2$ and CO_2 flux over 16 years (Fig. 5) showed some similarities to previous trend assessments in the South Atlantic Ocean (Landschützer et al., 2016). Our results indicated a lower number of significant trends however, since uncertainties in the trend analysis were accounted for. The uncertainties in both the $p\text{CO}_2$ (sw) estimates from extrapolation techniques and the gas transfer coefficient are rarely propagated through previous trend analyses. By accounting for these uncertainties, the trend analyses provide a robust depiction of regions that can confidently be determined as changing. As with the seasonal and inter-annual analysis, the CO_2 flux-based trend analysis showed a greater spatial area of significant trends, when compared to $\Delta p\text{CO}_2$, while regions also showed differing magnitudes between the $\Delta p\text{CO}_2$ and the CO_2 flux trends (Fig. 5).

The strongest trends in $\Delta p\text{CO}_2$ and the CO_2 flux were observed in the Benguela upwelling system. Arnone et al. (2017) reported positive trends in *in situ* $p\text{CO}_2$ (sw) of $6.1 \pm 1.4 \mu\text{atm yr}^{-1}$, between 2005 and 2015. Assuming an atmospheric CO_2 increase of $1.5 \mu\text{atm yr}^{-1}$ (Takahashi et al., 2002; Zeng et al., 2014), these results are consistent with the $\Delta p\text{CO}_2$ trends observed in this study ($1.5 - 3.8 \mu\text{atm yr}^{-1}$, Fig. 5a). Arnone et al. (2017) also suggested that the positive trend was due to a stronger influence of upwelling (Rouault et al., 2010), which injects CO_2 and nutrients into the upwelling system, that are not completely removed by enhanced NPP/NCP. Varela et al. (2015) indicated an increase in the strength of the Benguela upwelling. By contrast, Lamont et al. (2018) showed no significant change in upwelling in the Southern Benguela but increases in the Northern Benguela which are consistent with our data highlighting an increasing efflux of CO_2 to the atmosphere (Fig. 5b). The CO_2 flux trends in this study ($0.03 - 0.09 \text{ mol m}^{-2} \text{ yr}^{-1}$, Fig. 5b) were also consistent with a $0.13 \pm 0.03 \text{ mol m}^{-2} \text{ yr}^{-1}$ trend in CO_2 flux observed by Arnone et al. (2017). An increase in the strength of the upwelling that injects CO_2 into the surface layer, will be driven by enhanced (upwelling-conductive) winds, that also enhance the gas transfer. This highlights the importance of studying long-term trends using the CO_2 flux, because the enhancement of these trends by meteorological conditions would not be observed by using $\Delta p\text{CO}_2$.

Offshore from the upwelling region negative $\Delta p\text{CO}_2$ and CO_2 flux trends were observed. Rubio et al. (2009) showed that mesoscale filaments and eddies propagate away from the upwelling front, transporting nutrients offshore into the South Atlantic gyre. Ford et al. (2021a) showed negative correlations between sea level height anomalies (SLHA), and NPP/NCP anomalies (negative SLHA; positive NCP/NPP), indicating an influence of mesoscale features on $\Delta p\text{CO}_2$ and the CO_2 flux. Xiu et al. (2018) indicated that an increase in upwelling conducive winds could increase the number of mesoscale eddies, which would transport nutrients offshore of the Californian upwelling. Although the Benguela and Californian upwelling systems are not identical, these connections could suggest an elevated nutrient export offshore, driving elevated NPP/NCP, which would increase the CO_2 sink. Kulk et al. (2020) showed significant increases in NPP of $\sim 2 \% \text{ yr}^{-1}$, between 1998 and 2018 in the region of strong negative trends in the CO_2 flux observed in this study, that would reinforce the important biological contribution to long-term trends in the CO_2 flux.



The Equatorial Atlantic also indicated positive $\Delta p\text{CO}_2$ and CO_2 flux trends. Lefèvre et al. (2016) suggested a negative trend in *in situ* $\Delta p\text{CO}_2$, between 2006 and 2013, in the Eastern Equatorial Atlantic but indicated that the trend may be biased by extreme events at either end of the record. Parard et al. (2010) indicated a greater increase in *in situ* $p\text{CO}_2(\text{sw})$ than $p\text{CO}_2(\text{atm})$ (increasing $\Delta p\text{CO}_2$) between 1995 and 2007, however this trend was derived from only two cruises. An increase in $\Delta p\text{CO}_2$ is counter intuitive for the Equatorial upwelling where $\Delta p\text{CO}_2$ would in theory decrease with increasing $p\text{CO}_2(\text{atm})$, assuming a constant deep water CO_2 concentration. This could suggest a missing mechanism within the SA-FNN to estimate $p\text{CO}_2(\text{sw})$, such as changes in the biological export efficiency (Kim et al., 2019), which could suppress upwelling induced CO_2 outgassing.

The Western Tropical Atlantic, in the vicinity of the Amazon Plume, also showed positive $\Delta p\text{CO}_2$ and CO_2 flux trends. Previous studies have not investigated the $\Delta p\text{CO}_2$ or CO_2 flux trends in the Amazon Plume, however the carbon retention in a colored ocean site (CARIACO), situated to the northwest, displayed positive trends in $p\text{CO}_2(\text{sw})$ of $2.95 \pm 0.43 \mu\text{atm yr}^{-1}$ (Bates et al., 2014). Although, the air-sea CO_2 flux and $\Delta p\text{CO}_2$ within the Amazon Plume region is spatially and temporally variable (Bruto et al., 2017; Ibánhez et al., 2016; Valerio et al., 2021).

The South Atlantic gyre showed negative trends in $\Delta p\text{CO}_2$ and the CO_2 flux indicating an increasing drawdown of atmospheric CO_2 into the ocean, which were consistent with Landschützer et al. (2016) over the period from 1982 and 2011. Fay and Mckinley (2013) showed weak negative trends in $\Delta p\text{CO}_2$ using *in situ* observations over different time series lengths. Gregor et al. (2019), with an ensemble of complete $p\text{CO}_2(\text{sw})$ fields, indicated negative trends in $\Delta p\text{CO}_2$ however there was low confidence in these trends especially in the South Atlantic gyre. In contrast, Kitidis et al. (2017) reported a mean trend in *in situ* $\Delta p\text{CO}_2$ that was not significantly different from zero between 1995 and 2013. These contradictory trends support the conclusion that $\Delta p\text{CO}_2$ is unlikely to be representative of the CO_2 flux on interannual timescales. Therefore, we recommend that the CO_2 flux should be used to assess long-term variability in the oceanic CO_2 sink, as the importance of changes in solubility and surface turbulence (estimated via wind speed) increases.

The Integrated Ocean Carbon Research (IOC-R) highlights the role of biology in the global ocean CO_2 sink, and how it is changing as a key issue (Aricò et al., 2021) to address with the onset of the United Nations decade of ocean science (2021-2030). The biological contribution to interannual and long-term variations in the South Atlantic air-sea CO_2 flux shown in this study, and reinforced by Ford et al. (2022), indicates that the biology in the oceans cannot be assumed to be in steady state. Therefore, the biological effect on $\Delta p\text{CO}_2$ and CO_2 flux should not be overlooked when assessing the interannual and long-term variations in the global ocean carbon sink.

5. Conclusions

In this paper, we have identified the seasonal and interannual drivers of $\Delta p\text{CO}_2$ and the air-sea CO_2 flux in the South Atlantic Ocean using satellite observations. Seasonally, our results indicated that the subtropics were controlled by SST, and the subpolar regions were correlated with biological processes. Deviations from this trend occurred in the Benguela upwelling



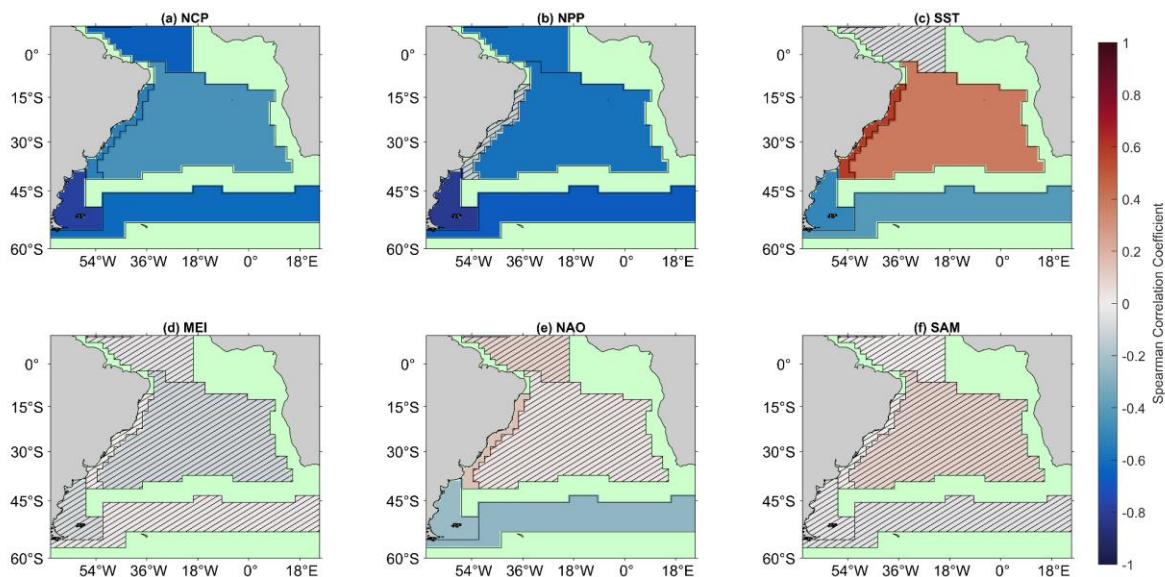
375 where predominately biological processes correlated with the $\Delta p\text{CO}_2$ variability, alongside upwelling. The Equatorial
Atlantic showed spatially variable drivers associated with the Amazon Plume and Equatorial upwelling which induced a
biological effect. These regions imply a strong biological control on $\Delta p\text{CO}_2$ through local physical processes. The CO_2 flux
had similar seasonal drivers to $\Delta p\text{CO}_2$, but with significant correlations over a larger spatial area. This highlights that $\Delta p\text{CO}_2$
can be used to indicate the important drivers of the CO_2 flux on seasonal timescales, but it's still possible that $\Delta p\text{CO}_2$ will
380 miss some of the spatial correlations and will likely overestimate the strength of any correlations.

Interannual variability of $\Delta p\text{CO}_2$ and the CO_2 flux was correlated with the MEI through a reduction (increase) of NCP and
increase (decrease) in SST during El Niño (La Niña) events, highlighting the important biological contribution to interannual
variability. The CO_2 flux responses extended over a larger geographical region, indicating that the CO_2 flux should be used
to assess interannual trends in the oceanic CO_2 sink, as opposed to a proxy such as $\Delta p\text{CO}_2$, which may overestimate the
385 strength of correlations and not include variability in the solubility and the gas transfer (estimated via wind speed). The 16
year trends in $\Delta p\text{CO}_2$ and the CO_2 flux were determined with associated uncertainties which identified negative trends in the
 CO_2 flux in the South Atlantic gyre. Positive trends in the CO_2 flux were observed in the Benguela upwelling region,
associated with an increase in the strength and frequency of upwelling. A transition to negative trends offshore were
consistent with elevated nutrient export from the upwelling front, and subsequent biological drawdown of CO_2 . These results
390 highlight that changes in biological activity within the South Atlantic Ocean control the interannual and long-term trends in
the oceanic CO_2 flux, and reinforce the importance of biology when assessing the global ocean carbon sink.

Appendices

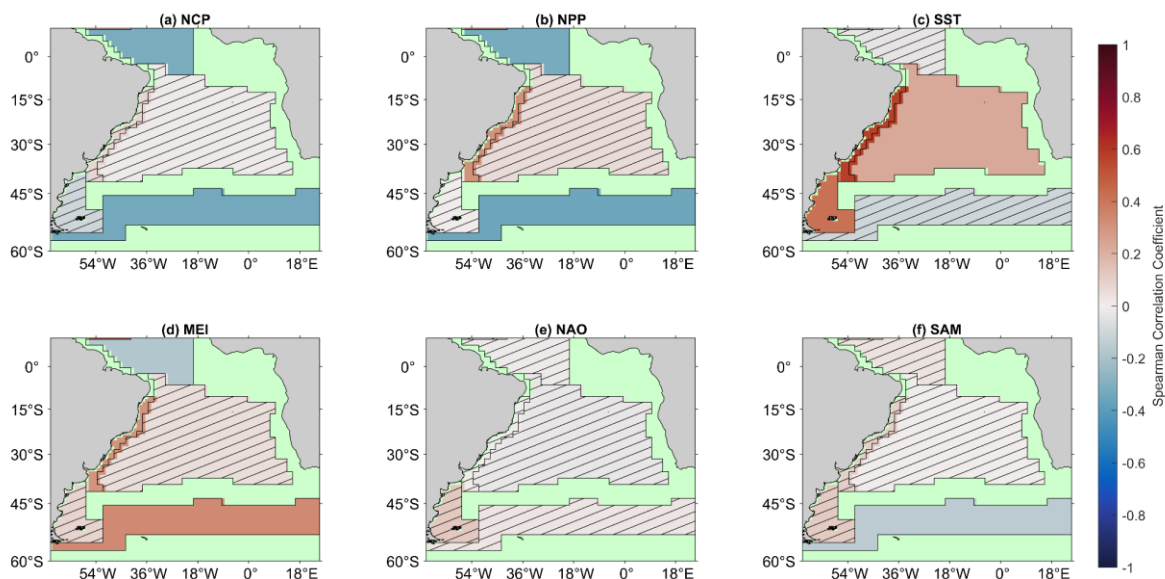
Appendix A – Driver analysis using *in situ* $\Delta p\text{CO}_2$

Henson et al. (2018) performed the X-11 analysis using *in situ* $p\text{CO}_2$ (_{sw}) observations to estimate average $\Delta p\text{CO}_2$ for the
395 Longhurst provinces (Longhurst, 1998). The *in situ* $p\text{CO}_2$ (_{sw}) observations were obtained from SOCATv2020
(<https://www.socat.info/>; Bakker et al., 2016), and were reanalysed to a consistent temperature and depth dataset (Reynolds
et al., 2002) using the 'fe_reanalyse_socat.py' package within FluxEngine (Holding et al., 2019; Shutler et al., 2016), which
follows the methodology of Goddijn-Murphy et al. (2015). $\Delta p\text{CO}_2$ was calculated using the reanalysed *in situ* $p\text{CO}_2$ (_{sw})
observations and $p\text{CO}_2$ (_{atm}). These $\Delta p\text{CO}_2$ estimates were used within the driver analysis as described by Henson et al.
400 (2018), using the drivers described in section 2.4, for the South Atlantic Longhurst provinces (Longhurst, 1998). The
seasonal drivers of *in situ* $\Delta p\text{CO}_2$ (Fig. A1) showed a similar spatial distribution as the SA-FNN $\Delta p\text{CO}_2$ (Fig. 1). The
interannual drivers (Fig. A2) showed some differences to the SA-FNN (Fig. 3). The averaging required to produce the *in situ*
 $\Delta p\text{CO}_2$ timeseries may mask interannual signals, and Ford et al. (2021a) indicated that averaging over large province areas
could mask correlations, especially in dynamic regions, and locally these correlations may be significant.



405

Figure A1 - Spearman correlations between the *in situ* $\Delta p\text{CO}_2$ seasonal component of the X-11 analysis and (a) net community production, (b) net primary production, (c) sea surface temperature, (d) Multivariate ENSO index, (e) North Atlantic Oscillation and (f) Southern Annular Mode seasonal components on a per province basis. Hashed areas indicate no significant correlations, and green regions indicate no analysis was performed due to missing data.



410

Figure A2 - Spearman correlations between the *in situ* $\Delta p\text{CO}_2$ interannual component of the X-11 analysis and (a) net community production, (b) net primary production, (c) sea surface temperature, (d) Multivariate ENSO index, (e) North Atlantic Oscillation



and (f) Southern Annular Mode interannual components on a per province basis. Hashed areas indicate no significant correlations, and green regions indicate no analysis was performed due to missing data.

415 **Data Availability**

Moderate Resolution Imaging Spectroradiometer on Aqua (MODIS-A) estimates of chlorophyll-a (NASA OBPG, 2017a), photosynthetically active radiation (NASA OBPG, 2017b) and sea surface temperature (NASA OBPG, 2015) are available from the National Aeronautics Space Administration (NASA) ocean colour website (<https://oceancolor.gsfc.nasa.gov/>). Modelled sea surface salinity from the Copernicus Marine Environment Modelling Service global ocean physics reanalysis product (GLORYS12V1) are available from CMEMS (CMEMS, 2021). ERA5 monthly reanalysis wind speeds are available from the Copernicus Climate Data Store (Hersbach et al., 2019). $p\text{CO}_2$ (atm) data are available from v5.5 of the global estimates of $p\text{CO}_2$ (sw) dataset (Landschützer et al., 2016, 2017). $p\text{CO}_2$ (sw) estimates generated by the SA-FNN are available from Pangaea (Ford et al., 2021b). SOCATv2020 *in situ* $p\text{CO}_2$ (sw) observations (Bakker et al., 2016) are available from <https://www.socat.info/index.php/version-2020/>.

425 **Author Contributions**

DJF, GHT, JDS and VK conceived and directed the research. DJF developed the code and prepared the manuscript. GHT, JDS and VK provided comments that shaped the final manuscript.

Competing Interests

The authors declare that they have no conflict of interest.

430 **Acknowledgements**

Daniel J. Ford was supported by a NERC GW4+ Doctoral Training Partnership studentship from the UK Natural Environment Research Council (NERC; NE/L002434/1). Gavin H. Tilstone and Vassilis Kitidis were supported by the AMT4CO₂Flux (4000125730/18/NL/FF/gp) contract from the European Space Agency and by the NERC National Capability funding to Plymouth Marine Laboratory for the Atlantic Meridional Transect (CLASS-AMT). The Atlantic Meridional Transect is funded by the UK Natural Environment Research Council through its National Capability Long-term Single Centre Science Programme, Climate Linked Atlantic Sector Science (grant number NE/R015953/1). This study contributes to the international IMBeR project and is contribution number 372 of the AMT programme. We also thank the Natural Environment Research Council Earth Observation Data Acquisition and Analysis Service (NEODAAS) for use of the Linux cluster to process the MODIS-A satellite imagery.



440 The Surface Ocean CO₂ Atlas (SOCAT) is an international effort, endorsed by the International Ocean Carbon Coordination Project (IOCCP), the Surface Ocean Lower Atmosphere Study (SOLAS) and the Integrated Marine Biosphere Research (IMBeR) program, to deliver a uniformly quality-controlled surface ocean CO₂ database. The many researchers and funding agencies responsible for the collection of data and quality control are thanked for their contributions to SOCAT.

445 **References**

- Aricò, S., Arrieta, J. M., Bakker, D. C. E., Boyd, P. W., Cotrim da Cunha, L., Chai, F., Dai, M., Gruber, N., Isensee, K., Ishii, M., Jiao, N., Lauvset, S. K., McKinley, G. A., Monteiro, P., Robinson, C., Sabine, C., Sanders, R., Schoo, K. L., Schuster, U., Shutler, J. D., Thomas, H., Wanninkhof, R., Watson, A. J., Bopp, L., Boss, E., Bracco, A., Cai, W., Fay, A., Feely, R. A., Gregor, L., Hauck, J., Heinze, C., Henson, S., Hwang, J., Post, J., Suntharalingam, P., Telszewski, M.,
- 450 Tilbrook, B., Valsala, V. and Rojas, A.: Integrated Ocean Carbon Research: A Summary of Ocean Carbon Research, and Vision of Coordinated Ocean Carbon Research and Observations for the Next Decade., edited by R. Wanninkhof, C. Sabine, and S. Aricò, UNESCO, Paris., 2021.
- Arnone, V., González-Dávila, M. and Magdalena Santana-Casiano, J.: CO₂ fluxes in the South African coastal region, *Mar. Chem.*, 195(July), 41–49, doi:10.1016/j.marchem.2017.07.008, 2017.
- 455 Bakker, D. C. E., Pfeil, B., Landa, C. S., Metzl, N., O'Brien, K. M., Olsen, A., Smith, K., Cosca, C., Harasawa, S., Jones, S. D., Nakaoka, S. I., Nojiri, Y., Schuster, U., Steinhoff, T., Sweeney, C., Takahashi, T., Tilbrook, B., Wada, C., Wanninkhof, R., Alin, S. R., Balestrini, C. F., Barbero, L., Bates, N. R., Bianchi, A. A., Bonou, F., Boutin, J., Bozec, Y., Burger, E. F., Cai, W. J., Castle, R. D., Chen, L., Chierici, M., Currie, K., Evans, W., Featherstone, C., Feely, R. A., Fransson, A., Goyet, C., Greenwood, N., Gregor, L., Hankin, S., Hardman-Mountford, N. J., Harlay, J., Hauck, J., Hoppema, M., Humphreys, M.
- 460 P., Hunt, C. W., Huss, B., Ibáñez, J. S. P., Johannessen, T., Keeling, R., Kitidis, V., Körtzinger, A., Kozyr, A., Krasakopoulou, E., Kuwata, A., Landschützer, P., Lauvset, S. K., Lefèvre, N., Lo Monaco, C., Manke, A., Mathis, J. T., Merlivat, L., Millero, F. J., Monteiro, P. M. S., Munro, D. R., Murata, A., Newberger, T., Omar, A. M., Ono, T., Paterson, K., Pearce, D., Pierrot, D., Robbins, L. L., Saito, S., Salisbury, J., Schlitzer, R., Schneider, B., Schweitzer, R., Sieger, R., Skjelvan, I., Sullivan, K. F., Sutherland, S. C., Sutton, A. J., Tadokoro, K., Telszewski, M., Tuma, M., Van Heuven, S. M. A.
- 465 C., Vandemark, D., Ward, B., Watson, A. J. and Xu, S.: A multi-decade record of high-quality fCO₂ data in version 3 of the Surface Ocean CO₂ Atlas (SOCAT), *Earth Syst. Sci. Data*, 8(2), 383–413, doi:10.5194/essd-8-383-2016, 2016.
- Bates, N. R., Astor, Y. M., Church, M. J., Currie, K., Dore, J. E., González-Dávila, M., Lorenzoni, L., Muller-Karger, F., Olafsson, J. and Santana-Casiano, J. M.: A time-series view of changing surface ocean chemistry due to ocean uptake of anthropogenic CO₂ and ocean acidification, *Oceanography*, 27(1), 126–141, doi:10.5670/oceanog.2014.16, 2014.
- 470 Bonou, F. K., Noriega, C., Lefèvre, N. and Araujo, M.: Distribution of CO₂ parameters in the Western Tropical Atlantic Ocean, *Dyn. Atmos. Ocean.*, 73, 47–60, doi:10.1016/j.dynatmoce.2015.12.001, 2016.



- Bruto, L., Araujo, M., Noriega, C., Veleda, D. and Lefèvre, N.: Variability of CO₂ fugacity at the western edge of the tropical Atlantic Ocean from the 8°N to 38°W PIRATA buoy, *Dyn. Atmos. Ocean.*, 78, 1–13, doi:10.1016/j.dynatmoce.2017.01.003, 2017.
- 475 CMEMS: Copernicus Marine Modelling Service global ocean physics reanalysis product (GLORYS12V1), Copernicus Mar. Model. Serv. [data set], doi:10.48670/moi-00021, 2021.
- Colberg, F., Reason, C. J. C. and Rodgers, K.: South Atlantic response to El Niño-Southern Oscillation induced climate variability in an ocean general circulation model, *J. Geophys. Res. C Ocean.*, 109(12), 1–14, doi:10.1029/2004JC002301, 2004.
- 480 Cooley, S. R., Coles, V. J., Subramaniam, A. and Yager, P. L.: Seasonal variations in the Amazon plume-related atmospheric carbon sink, *Global Biogeochem. Cycles*, 21(3), 1–15, doi:10.1029/2006GB002831, 2007.
- Dickson, A. G., Sabine, C. L. and Christian, J. R.: Guide to Best Practices for Ocean CO₂ measurements., 2007.
- Dong, Y., Yang, M., Bakker, D. C. E., Kitidis, V. and Bell, T. G.: Uncertainties in eddy covariance air–sea CO₂ flux measurements and implications for gas transfer velocity parameterisations, *Atmos. Chem. Phys.*, 21(10), 8089–8110, doi:10.5194/acp-21-8089-2021, 2021.
- 485 Donlon, C. J., Nightingale, T. J., Sheasby, T., Turner, J., Robinson, I. S. and Emery, W. J.: Implications of the oceanic thermal skin temperature deviation at high wind speed, *Geophys. Res. Lett.*, 26(16), 2505–2508, doi:10.1029/1999GL900547, 1999.
- Fay, A. R. and McKinley, G. A.: Global trends in surface ocean pCO₂ from in situ data, *Global Biogeochem. Cycles*, 27(2), 541–557, doi:10.1002/gbc.20051, 2013.
- 490 Fogt, R. L., Bromwich, D. H. and Hines, K. M.: Understanding the SAM influence on the South Pacific ENSO teleconnection, *Clim. Dyn.*, 36(7), 1555–1576, doi:10.1007/s00382-010-0905-0, 2011.
- Ford, D., Tilstone, G. H., Shutler, J. D., Kitidis, V., Lobanova, P., Schwarz, J., Poulton, A. J., Serret, P., Lamont, T., Chuqui, M., Barlow, R., Lozano, J., Kampel, M. and Brandini, F.: Wind speed and mesoscale features drive net autotrophy in the South Atlantic Ocean, *Remote Sens. Environ.*, 260, 112435, doi:10.1016/j.rse.2021.112435, 2021a.
- 495 Ford, D. J., Tilstone, G. H., Shutler, J. D. and Kitidis, V.: Interpolated surface ocean carbon dioxide partial pressure for the South Atlantic Ocean (2002–2018) using different biological parameters, PANGAEA [data set], doi:10.1594/PANGAEA.935936, 2021b.
- Ford, D. J., Tilstone, G. H., Shutler, J. D. and Kitidis, V.: Derivation of seawater CO₂ from net community production identifies the South Atlantic Ocean as a CO₂ source, *Biogeosciences*, 19(1), 93–115, doi:10.5194/bg-19-93-2022, 2022.
- 500 Friedlingstein, P., O’Sullivan, M., Jones, M. W., Andrew, R. M., Hauck, J., Olsen, A., Peters, G. P., Peters, W., Pongratz, J., Sitch, S., Le Quéré, C., Canadell, J. G., Ciais, P., Jackson, R. B., Alin, S., Aragão, L. E. O. C., Arneeth, A., Arora, V., Bates, N. R., Becker, M., Benoit-Cattin, A., Bittig, H. C., Bopp, L., Bultan, S., Chandra, N., Chevallier, F., Chini, L. P., Evans, W., Florentie, L., Forster, P. M., Gasser, T., Gehlen, M., Gilfillan, D., Gkritzalis, T., Gregor, L., Gruber, N., Harris, I., Hartung, K., Haverd, V., Houghton, R. A., Ilyina, T., Jain, A. K., Joetzer, E., Kadono, K., Kato, E., Kitidis, V., Korsbakken, J. I.,
- 505



- Landschützer, P., Lefèvre, N., Lenton, A., Lienert, S., Liu, Z., Lombardozzi, D., Marland, G., Metzl, N., Munro, D. R., Nabel, J. E. M. S., Nakaoka, S.-I., Niwa, Y., O'Brien, K., Ono, T., Palmer, P. I., Pierrot, D., Poulter, B., Resplandy, L., Robertson, E., Rödenbeck, C., Schwinger, J., Séférian, R., Skjelvan, I., Smith, A. J. P., Sutton, A. J., Tanhua, T., Tans, P. P., Tian, H., Tilbrook, B., van der Werf, G., Vuichard, N., Walker, A. P., Wanninkhof, R., Watson, A. J., Willis, D., Wiltshire, A. J., Yuan, W., Yue, X. and Zaehle, S.: Global Carbon Budget 2020, *Earth Syst. Sci. Data*, 12(4), 3269–3340, doi:10.5194/essd-12-3269-2020, 2020.
- Goddijn-Murphy, L. M., Woolf, D. K., Land, P. E., Shutler, J. D. and Donlon, C.: The OceanFlux Greenhouse Gases methodology for deriving a sea surface climatology of CO₂ fugacity in support of air-sea gas flux studies, *Ocean Sci.*, 11(4), 519–541, doi:10.5194/os-11-519-2015, 2015.
- 515 González-Dávila, M., Santana-Casiano, J. M. and Ucha, I. R.: Seasonal variability of fCO₂ in the Angola-Benguela region, *Prog. Oceanogr.*, 83(1–4), 124–133, doi:10.1016/j.pcean.2009.07.033, 2009.
- Gregor, L., Lebehot, A. D., Kok, S. and Scheel Monteiro, P. M.: A comparative assessment of the uncertainties of global surface ocean CO₂ estimates using a machine-learning ensemble (CSIR-ML6 version 2019a)-Have we hit the wall?, *Geosci. Model Dev.*, 12(12), 5113–5136, doi:10.5194/gmd-12-5113-2019, 2019.
- 520 Henson, S. A., Humphreys, M. P., Land, P. E., Shutler, J. D., Goddijn-Murphy, L. and Warren, M.: Controls on Open-Ocean North Atlantic ΔpCO₂ at Seasonal and Interannual Time Scales Are Different, *Geophys. Res. Lett.*, 45(17), 9067–9076, doi:10.1029/2018GL078797, 2018.
- Hersbach, H., Bell, B., Berrisford, P., Biavati, G., Horányi, A., Muñoz Sabater, J., Nicolas, J., Peubey, C., Radu, R., Rozum, I., Schepers, D., Simmons, A., Soci, C., Dee, D. and Thépaut, J.-N.: ERA5 monthly averaged data on single levels from 1979 to present, *Copernicus Clim. Chang. Serv. Clim. Data Store [dataset]*, doi:10.24381/cds.f17050d7, 2019.
- 525 Ho, D. T., Law, C. S., Smith, M. J., Schlosser, P., Harvey, M. and Hill, P.: Measurements of air-sea gas exchange at high wind speeds in the Southern Ocean: Implications for global parameterizations, *Geophys. Res. Lett.*, 33(16), L16611, doi:10.1029/2006GL026817, 2006.
- 530 Holding, T., Ashton, I. G., Shutler, J. D., Land, P. E., Nightingale, P. D., Rees, A. P., Brown, I., Piolle, J.-F., Kock, A., Bange, H. W., Woolf, D. K., Goddijn-Murphy, L., Pereira, R., Paul, F., Girard-Arduin, F., Chapron, B., Rehder, G., Arduin, F. and Donlon, C. J.: The FluxEngine air-sea gas flux toolbox: simplified interface and extensions for in situ analyses and multiple sparingly soluble gases, *Ocean Sci.*, 15(6), 1707–1728, doi:10.5194/os-15-1707-2019, 2019.
- Hopkins, J., Lucas, M., Dufau, C., Sutton, M., Stum, J., Lauret, O. and Channelliere, C.: Detection and variability of the Congo River plume from satellite derived sea surface temperature, salinity, ocean colour and sea level, *Remote Sens. Environ.*, 139, 365–385, doi:10.1016/j.rse.2013.08.015, 2013.
- 535 Hu, C., Lee, Z. and Franz, B.: Chlorophyll a algorithms for oligotrophic oceans: A novel approach based on three-band reflectance difference, *J. Geophys. Res. Ocean.*, 117(1), 1–25, doi:10.1029/2011JC007395, 2012.
- Ibáñez, J. S. P., Araujo, M. and Lefèvre, N.: The overlooked tropical oceanic CO₂ sink, *Geophys. Res. Lett.*, 43(8), 3804–3812, doi:10.1002/2016GL068020, 2016.



- 540 IPCC: Climate Change 2021: The Physical Science Basis. Contribution of Working Group I to the Sixth Assessment Report of the Intergovernmental Panel on Climate Change, edited by V. Masson-Delmotte, P. Zhai, A. Pirani, S. L. Connors, C. Péan, S. Berger, N. Caud, Y. Chen, L. Goldfarb, M. I. Gomis, M. Huang, K. Leitzell, E. Lonnoy, J. B. R. Matthews, T. K. Maycock, T. Waterfield, O. Yelekçi, R. Yu, and B. Zhou, Cambridge University Press., 2021.
Kendall, M. G.: Rank Correlation Methods, 4th ed., Charles Griffin, London, UK., 1975.
- 545 Keppler, L. and Landschützer, P.: Regional Wind Variability Modulates the Southern Ocean Carbon Sink, *Sci. Rep.*, 9(1), 1–10, doi:10.1038/s41598-019-43826-y, 2019.
Kim, H. J., Kim, T., Hyeong, K., Yeh, S., Park, J., Yoo, C. M. and Hwang, J.: Suppressed CO₂ Outgassing by an Enhanced Biological Pump in the Eastern Tropical Pacific, *J. Geophys. Res. Ocean.*, 124(11), 7962–7973, doi:10.1029/2019JC015287, 2019.
- 550 Kitidis, V., Brown, I., Hardman-mountford, N. and Lefèvre, N.: Surface ocean carbon dioxide during the Atlantic Meridional Transect (1995 – 2013); evidence of ocean acidification, *Prog. Oceanogr.*, 158, 65–75, doi:10.1016/j.pocean.2016.08.005, 2017.
Körtzinger, A.: A significant CO₂ sink in the tropical Atlantic Ocean associated with the Amazon River plume, *Geophys. Res. Lett.*, 30(24), 2–5, doi:10.1029/2003GL018841, 2003.
- 555 Kulk, G., Platt, T., Dingle, J., Jackson, T., Jönsson, B. F., Bouman, H. A., Babin, M., Brewin, R. J. W., Doblin, M., Estrada, M., Figueiras, F. G., Furuya, K., González-Benítez, N., Gudfinnsson, H. G., Gudmundsson, K., Huang, B., Isada, T., Kovač, Ž., Lutz, V. A., Marañón, E., Raman, M., Richardson, K., Rozema, P. D., van de Poll, W. H., Segura, V., Tilstone, G. H., Uitz, J., van Dongen-Vogels, V., Yoshikawa, T. and Sathyendranath, S.: Primary production, an index of climate change in the ocean: Satellite-based estimates over two decades, *Remote Sens.*, 12(5), doi:10.3390/rs12050826, 2020.
- 560 Lamont, T., Barlow, R. G. and Kyewalyanga, M. S.: Physical drivers of phytoplankton production in the southern Benguela upwelling system, *Deep. Res. Part I Oceanogr. Res. Pap.*, 90(1), 1–16, doi:10.1016/j.dsr.2014.03.003, 2014.
Lamont, T., García-Reyes, M., Bograd, S. J., van der Lingen, C. D. and Sydeman, W. J.: Upwelling indices for comparative ecosystem studies: Variability in the Benguela Upwelling System, *J. Mar. Syst.*, 188, 3–16, doi:10.1016/j.jmarsys.2017.05.007, 2018.
- 565 Landschützer, P., Gruber, N., Bakker, D. C. E., Schuster, U., Nakaoka, S., Payne, M. R., Sasse, T. P. and Zeng, J.: A neural network-based estimate of the seasonal to inter-annual variability of the Atlantic Ocean carbon sink, *Biogeosciences*, 10(11), 7793–7815, doi:10.5194/bg-10-7793-2013, 2013.
Landschützer, P., Gruber, N., Bakker, D. C. E. and Schuster, U.: Recent variability of the global ocean carbon sink, *Global Biogeochem. Cycles*, 28(9), 927–949, doi:10.1002/2014GB004853, 2014.
- 570 Landschützer, P., Gruber, N., Haumann, F. A., Rödenbeck, C., Bakker, D. C. E., van Heuven, S., Hoppema, M., Metzl, N., Sweeney, C., Takahashi, T., Tilbrook, B. and Wanninkhof, R.: The reinvigoration of the Southern Ocean carbon sink, *Science (80-.)*, 349(6253), 1221–1224, doi:10.1126/science.aab2620, 2015.
Landschützer, P., Gruber, N. and Bakker, D. C. E.: Decadal variations and trends of the global ocean carbon sink, *Global*



- Biogeochem. Cycles, 30(10), 1396–1417, doi:10.1002/2015GB005359, 2016.
- 575 Landschützer, P., Gruber, N. and Bakker, D. C. E.: An observation-based global monthly gridded sea surface pCO₂ product from 1982 onward and its monthly climatology (NCEI Accession 0160558), NOAA Natl. Centers Environ. Information. Dataset, doi:10.7289/v5z899n6, 2017.
- Lefèvre, N., Diverrés, D. and Gallois, F.: Origin of CO₂ undersaturation in the western tropical Atlantic, *Tellus, Ser. B Chem. Phys. Meteorol.*, 62(5), 595–607, doi:10.1111/j.1600-0889.2010.00475.x, 2010.
- 580 Lefèvre, N., Guillot, A., Beaumont, L. and Danguy, T.: Variability of fCO₂ in the Eastern Tropical Atlantic from a moored buoy, *J. Geophys. Res. Ocean.*, 113(1), doi:10.1029/2007JC004146, 2008.
- Lefèvre, N., Caniaux, G., Janicot, S. and Gueye, A. K.: Increased CO₂ outgassing in February–May 2010 in the tropical Atlantic following the 2009 Pacific El Niño, *J. Geophys. Res. Ocean.*, 118(4), 1645–1657, doi:10.1002/jgrc.20107, 2013.
- Lefèvre, N., Veleda, D., Araujo, M. and Caniaux, G.: Variability and trends of carbon parameters at a time series in the eastern tropical Atlantic, *Tellus, Ser. B Chem. Phys. Meteorol.*, 68(1), doi:10.3402/tellusb.v68.30305, 2016.
- 585 Lefèvre, N., Tyaquicã, P., Veleda, D., Perruche, C. and van Gennip, S. J.: Amazon River propagation evidenced by a CO₂ decrease at 8°N, 38°W in September 2013, *J. Mar. Syst.*, 211(July), 103419, doi:10.1016/j.jmarsys.2020.103419, 2020.
- Lefèvre, N., Mejia, C., Khvorostyanov, D., Beaumont, L. and Koffi, U.: Ocean Circulation Drives the Variability of the Carbon System in the Eastern Tropical Atlantic, *Oceans*, 2(1), 126–148, doi:10.3390/oceans2010008, 2021.
- 590 Longhurst, A.: *Ecological geography of the sea*, Academic Press, San Diego., 1998.
- Mann, H. B.: Nonparametric Tests Against Trend, *Econometrica*, 13(3), 245, doi:10.2307/1907187, 1945.
- Morel, A.: Light and marine photosynthesis: a spectral model with geochemical and climatological implications, *Prog. Oceanogr.*, 26(3), 263–306, doi:10.1016/0079-6611(91)90004-6, 1991.
- NASA OBPG: MODIS Aqua Level 3 SST Thermal IR Daily 4km Daytime v2014.0, NASA Phys. Oceanogr. DAAC [data set], doi:10.5067/MODSA-1D4D4, 2015.
- 595 NASA OBPG: MODIS-Aqua Level 3 Mapped Chlorophyll Data Version R2018.0, NASA Ocean Biol. DAAC [data set], doi:10.5067/AQUA/MODIS/L3M/CHL/2018, 2017a.
- NASA OBPG: MODIS-Aqua Level 3 Mapped Photosynthetically Available Radiation Data Version R2018.0, NASA Ocean Biol. DAAC [data set], doi:10.5067/AQUA/MODIS/L3M/PAR/2018, 2017b.
- 600 Nightingale, P. D., Malin, G., Law, C. S., Watson, A. J., Liss, P. S., Liddicoat, M. I., Boutin, J. and Upstill-Goddard, R. C.: In situ evaluation of air-sea gas exchange parameterizations using novel conservative and volatile tracers, *Global Biogeochem. Cycles*, 14(1), 373–387, doi:10.1029/1999GB900091, 2000.
- O’Reilly, J. E. and Werdell, P. J.: Chlorophyll algorithms for ocean color sensors - OC4, OC5 & OC6, *Remote Sens. Environ.*, 229(May), 32–47, doi:10.1016/j.rse.2019.04.021, 2019.
- 605 O’Reilly, J. E., Maritorena, S., Mitchell, B. G., Siegel, D. A., Carder, K. L., Garver, S. A., Kahru, M. and McClain, C.: Ocean color chlorophyll algorithms for SeaWiFS encompassing chlorophyll concentrations between, *J. Geophys. Res.*, 103(C11), 24937–24953, 1998.



- Parard, G., Lefèvre, N. and Boutin, J.: Sea water fugacity of CO₂ at the PIRATA mooring at 6°S, 10°W, *Tellus, Ser. B Chem. Phys. Meteorol.*, 62(5), 636–648, doi:10.1111/j.1600-0889.2010.00503.x, 2010.
- 610 Pezzulli, S., Stephenson, D. B. and Hannachi, A.: The variability of seasonality, *J. Clim.*, 18(1), 71–88, doi:10.1175/JCLI-3256.1, 2005.
- Radenac, M. H., Jouanno, J., Carine Tchamabi, C., Awo, M., Bourlès, B., Arnault, S. and Aumont, O.: Physical drivers of the nitrate seasonal variability in the Atlantic cold tongue, *Biogeosciences*, 17(2), 529–545, doi:10.5194/bg-17-529-2020, 2020.
- 615 Reboita, M. S., Ambrizzi, T., Silva, B. A., Pinheiro, R. F. and da Rocha, R. P.: The south atlantic subtropical anticyclone: Present and future climate, *Front. Earth Sci.*, 7(February), 1–15, doi:10.3389/feart.2019.00008, 2019.
- Reynolds, R. W., Rayner, N. A., Smith, T. M., Stokes, D. C. and Wang, W.: An improved in situ and satellite SST analysis for climate, *J. Clim.*, 15(13), 1609–1625, doi:10.1175/1520-0442(2002)015<1609:AIISAS>2.0.CO;2, 2002.
- Rodrigues, R. R., Campos, E. J. D. and Haarsma, R.: The impact of ENSO on the south Atlantic subtropical dipole mode, *J. Clim.*, 28(7), 2691–2705, doi:10.1175/JCLI-D-14-00483.1, 2015.
- 620 Rouault, M., Pohl, B. and Penven, P.: Coastal oceanic climate change and variability from 1982 to 2009 around South Africa, *African J. Mar. Sci.*, 32(2), 237–246, doi:10.2989/1814232x.2010.501563, 2010.
- Rubio, A., Blanke, B., Speich, S., Grima, N. and Roy, C.: Mesoscale eddy activity in the southern Benguela upwelling system from satellite altimetry and model data, *Prog. Oceanogr.*, 83(1–4), 288–295, doi:10.1016/j.pocean.2009.07.029, 625 2009.
- Sabine, C. L., Hankin, S., Koyuk, H., Bakker, D. C. E., Pfeil, B., Olsen, A., Metzl, N., Kozyr, A., Fassbender, A., Manke, A., Malczyk, J., Akl, J., Alin, S. R., Bellerby, R. G. J., Borges, A., Boutin, J., Brown, P. J., Cai, W. J., Chavez, F. P., Chen, A., Cosca, C., Feely, R. A., González-Dávila, M., Goyet, C., Hardman-Mountford, N., Heinze, C., Hoppema, M., Hunt, C. W., Hydes, D., Ishii, M., Johannessen, T., Key, R. M., Körtzinger, A., Landschützer, P., Lauvset, S. K., Lefèvre, N., Lenton, 630 A., Lourantou, A., Merlivat, L., Midorikawa, T., Mintrop, L., Miyazaki, C., Murata, A., Nakadate, A., Nakano, Y., Nakaoka, S., Nojiri, Y., Omar, A. M., Padin, X. A., Park, G. H., Paterson, K., Perez, F. F., Pierrot, D., Poisson, A., Ríos, A. F., Salisbury, J., Santana-Casiano, J. M., S. Sarma, V. V. S., Schlitzer, R., Schneider, B., Schuster, U., Sieger, R., Skjelvan, I., Steinhoff, T., Suzuki, T., Takahashi, T., Tedesco, K., Telszewski, M., Thomas, H., Tilbrook, B., Vandemark, D., Veness, T., Watson, A. J., Weiss, R., Wong, C. S. and Yoshikawa-Inoue, H.: Surface Ocean CO₂ Atlas (SOCAT) gridded data products, 635 *Earth Syst. Sci. Data*, 5(1), 145–153, doi:10.5194/essd-5-145-2013, 2013.
- Santana-Casiano, J. M., González-Dávila, M. and Ucha, I. R.: Carbon dioxide fluxes in the Benguela upwelling system during winter and spring: A comparison between 2005 and 2006, *Deep Sea Res. Part II Top. Stud. Oceanogr.*, 56(8–10), 533–541, doi:10.1016/j.dsr2.2008.12.010, 2009.
- Sen, P. K.: Estimates of the Regression Coefficient Based on Kendall’s Tau, *J. Am. Stat. Assoc.*, 63(324), 1379–1389, 640 doi:10.1080/01621459.1968.10480934, 1968.
- Shiskin, J., Young, A. J. and Musgrave, J. C.: The X-11 variant of the Census Method II Seasonal Adjustment Program, US



- Dept of Commerce., 1967.
- Shutler, J. D., Land, P. E., Piolle, J. F., Woolf, D. K., Goddijn-Murphy, L., Paul, F., Girard-Ardhuin, F., Chapron, B. and Donlon, C. J.: FluxEngine: A flexible processing system for calculating atmosphere-ocean carbon dioxide gas fluxes and climatologies, *J. Atmos. Ocean. Technol.*, 33(4), 741–756, doi:10.1175/JTECH-D-14-00204.1, 2016.
- 645 Smyth, T. J., Tilstone, G. H. and Groom, S. B.: Integration of radiative transfer into satellite models of ocean primary production, *J. Geophys. Res. C Ocean.*, 110(10), 1–11, doi:10.1029/2004JC002784, 2005.
- Takahashi, T., Sutherland, S. C., Sweeney, C., Poisson, A., Metz, N., Tilbrook, B., Bates, N., Wanninkhof, R., Feely, R. A., Sabine, C., Olafsson, J. and Nojiri, Y.: Global sea–air CO₂ flux based on climatological surface ocean pCO₂, and seasonal biological and temperature effects, *Deep Sea Res. Part II Top. Stud. Oceanogr.*, 49(9–10), 1601–1622, doi:10.1016/S0967-0645(02)00003-6, 2002.
- 650 Tilstone, G. H., Smyth, T. J., Gowen, R. J., Martinez-Vicente, V. and Groom, S. B.: Inherent optical properties of the Irish Sea and their effect on satellite primary production algorithms, *J. Plankton Res.*, 27(11), 1127–1148, doi:10.1093/plankt/fbi075, 2005.
- 655 Tilstone, G. H., Smyth, T., Poulton, A. and Hutson, R.: Measured and remotely sensed estimates of primary production in the Atlantic Ocean from 1998 to 2005, *Deep. Res. Part II Top. Stud. Oceanogr.*, 56(15), 918–930, doi:10.1016/j.dsr2.2008.10.034, 2009.
- Tilstone, G. H., Xie, Y. yuan, Robinson, C., Serret, P., Raitsos, D. E., Powell, T., Aranguren-Gassis, M., Garcia-Martin, E. E. and Kitidis, V.: Satellite estimates of net community production indicate predominance of net autotrophy in the Atlantic Ocean, *Remote Sens. Environ.*, 164, 254–269, doi:10.1016/j.rse.2015.03.017, 2015.
- 660 Valerio, A. M., Kampel, M., Ward, N. D., Sawakuchi, H. O., Cunha, A. C. and Richey, J. E.: CO₂ partial pressure and fluxes in the Amazon River plume using in situ and remote sensing data, *Cont. Shelf Res.*, 215(May 2020), 104348, doi:10.1016/j.csr.2021.104348, 2021.
- Vantrepotte, V. and Mélin, F.: Inter-annual variations in the SeaWiFS global chlorophyll a concentration (1997–2007), *Deep. Res. Part I Oceanogr. Res. Pap.*, 58(4), 429–441, doi:10.1016/j.dsr.2011.02.003, 2011.
- 665 Varela, R., Álvarez, I., Santos, F., DeCastro, M. and Gómez-Gesteira, M.: Has upwelling strengthened along worldwide coasts over 1982–2010?, *Sci. Rep.*, 5, 1–15, doi:10.1038/srep10016, 2015.
- Wanninkhof, R.: Relationship between wind speed and gas exchange over the ocean, *J. Geophys. Res.*, 12(C5), 351–362, doi:10.1029/92JC00188, 2014.
- 670 Watson, A. J., Schuster, U., Shutler, J. D., Holding, T., Ashton, I. G. C., Landschützer, P., Woolf, D. K. and Goddijn-Murphy, L.: Revised estimates of ocean-atmosphere CO₂ flux are consistent with ocean carbon inventory, *Nat. Commun.*, 11(1), 1–6, doi:10.1038/s41467-020-18203-3, 2020.
- Weiss, R. F.: Carbon dioxide in water and seawater: the solubility of a non-ideal gas, *Mar. Chem.*, 2(3), 203–215, doi:10.1016/0304-4203(74)90015-2, 1974.
- 675 Wilks, D. S.: On “field significance” and the false discovery rate, *J. Appl. Meteorol. Climatol.*, 45(9), 1181–1189,



doi:10.1175/JAM2404.1, 2006.

Woolf, D. K., Land, P. E., Shutler, J. D., Goddijn-Murphy, L. M. and Donlon, C. J.: On the calculation of air-sea fluxes of CO₂ in the presence of temperature and salinity gradients, *J. Geophys. Res. Ocean.*, 121(2), 1229–1248, doi:10.1002/2015JC011427, 2016.

680 Woolf, D. K., Shutler, J. D., Goddijn-Murphy, L., Watson, A. J., Chapron, B., Nightingale, P. D., Donlon, C. J., Piskozub, J., Yelland, M. J., Ashton, I., Holding, T., Schuster, U., Girard-Ardhuin, F., Grouazel, A., Piolle, J. F., Warren, M., Wrobel-Niedzwiecka, I., Land, P. E., Torres, R., Prytherch, J., Moat, B., Hanafin, J., Ardhuin, F. and Paul, F.: Key Uncertainties in the Recent Air-Sea Flux of CO₂, *Global Biogeochem. Cycles*, 33(12), 1548–1563, doi:10.1029/2018GB006041, 2019.

Xiong, X., Masuda, Y., Hashioka, T., Ono, T. and Yamanaka, Y.: Effect of seasonal change in gas transfer coefficient on air-sea CO₂ flux in the western North Pacific, *J. Oceanogr.*, 71(6), 685–701, doi:10.1007/s10872-015-0313-5, 2015.

685 Xiu, P., Chai, F., Curchitser, E. N. and Castruccio, F. S.: Future changes in coastal upwelling ecosystems with global warming: The case of the California Current System, *Sci. Rep.*, 8(1), 1–9, doi:10.1038/s41598-018-21247-7, 2018.

Zeng, J., Nojiri, Y., Landschützer, P., Telszewski, M. and Nakaoka, S.: A global surface ocean fCO₂ climatology based on a feed-forward neural network, *J. Atmos. Ocean. Technol.*, 31(8), 1838–1849, doi:10.1175/JTECH-D-13-00137.1, 2014.

690